ORIGINAL PAPER

CrossMark

Design and Characterization of Novel Potentially Biodegradable Triple-Shape Memory Polymers Based on Immiscible Poly(L-lactide)/Poly(ε-caprolactone) Blends

Fatemeh Khademeh Molavi[1,2] · Ismaeil Ghasemi[1] · Massimo Messori[2] · Masoud Esfandeh[1]

Abstract

In this study, covalently cross-linked network strategy has been applied to prepare new triple-shape memory polymers (TSPs) based on poly(L-lactide) (PLA)/poly(ε-caprolactone) (PCL) blends. The TSPs were fabricated by adding di-cumyl peroxide, with triallyl isocyanurate as a coagent for performing the cross-linking reaction. The differential scanning calorimetry (DSC) analysis demonstrated that all the PLA/PCL blends show two melting points ($T_{m,PCL}$ and $T_{m,PLA}$), which can be employed as the transition temperature (T_{trans}) to induce triple-shape memory behavior. The scanning electron microscopy (SEM) analysis indicated that there are two immiscible morphologies: co-continuous structure and matrix-droplet. The influence of temperature on the crystalline phase changes was analyzed by X-ray diffraction at various temperatures. The results revealed that during the heating–cooling cycle, the degree of crystallinity decreased when the temperature increased and at higher temperature, the crystallization peaks of PCL disappeared. Multiple thermal–mechanical tests were performed and the results showed that the composition ratio of the two phases plays an important role in the triple-shape memory behavior. The results confirmed that the excellent shape memory behavior was obtained for the sample containing 50 wt% PCL.

Keywords Triple-shape memory polymer · Smart materials · Potentially biodegradable blend · Thermo-mechanical cycle · Transition temperature

Introduction

The shape memory polymers (SMPs) are regarded as smart materials that are able to respond to an external stimulus, such as heat, light, magnet, or electricity and so on [1–5]. Thermally-induced SMPs are more common [6, 7]. Most of these polymers have a permanent shape provided by the physical or the chemical cross-linking network, which determines the fixed shape and can act as net-point, while the soft polymers a with suitable melting temperature or crystallization have a temporary shape and are responsible for shape recovery [8, 9]. In the other words, the transition temperature of a switch polymer is lower than that of the net-point, thus, the hard phases can act as the net-points, while the soft phases act as the switches [10, 11]. In general, for thermally-induced SMPs, the reversible thermal transition includes the glass transition temperature (T_g) [12, 13] or the melting temperature (T_m) [14–17].

Recently, the multiple-shape memory polymers (MSMPs) have attracted much attention because they can memorize two or more temporary shapes in one shape memory effect (SME) cycle [18–21]. The MSMPs can be created by incorporating two or more different thermal transitions in one system [22–24]. The first example of MSMPs can be traced to Lendlein and co-workers, who created the triple-shape memory polymer [19]. One of the first cross-linked MSMPs was Nafion, a cross-linked fluoropolymer with chemical functional groups and which was able to show the multiple-shape memory behavior due to several thermo-mechanical programming steps and the broad glass transition temperature [6, 25]. There are two well-known strategies for designing MSMPs. The first is to incorporate two or more thermal transitions (switching

✉ Ismaeil Ghasemi
I.ghasemi@ippi.ac.ir

1 Department of Polymer Processing, Iran Polymer and Petrochemical Institute, P. O. Box:14965/115, Tehran, Iran

2 Department of Engineering "Enzo Ferrari", University of Modena and Reggio Emilia, Via P. Vivarelli 10/1, 41125 Modena, Italy

temperatures) into the systems; the second is to introduce a broad glass transition temperature range [26, 27]. It is worthy to note that the multi-step fixation and recovery is the main reason for the creation of MSMPs based on at least two reversible phase transitions with well-separated hard and soft phase with different switching temperatures [27].

However, nowa-days, the renewable polymers have received extensive interest as an alternative to the traditional petroleum-based polymer because of the environmental problems the latter create [28–31]. Currently, there has been a great interest in the development of high-performance biodegradable polymers, such as polylactide (PLA), poly (ε-caprolactone) (PCL), starch, cellulose, and chitosan. They have been extensively used for a wide range of applications because of their thermoplastic, biodegradable, and biocompatible properties. Among them, PLA and PCL received special attention. They can be used in many fields, including their biological and medical applications as an alternative source of the commercial polymer [32, 33].

One of the simplest ways to prepare the MSMPs is by polymer blending [34]. The type of blends usually consists of amorphous and crystalline/semi-crystalline polymers. An effective strategy is to blend these polymers with many selective polymers. This is also a convenient way to obtain new materials which have high performance. Among them, the PLA-blend-PCL materials are very interesting because they are two biodegradable polymers with a large range of mechanical properties and biodegradability. In addition, when the rubbery PCL with a slow degradation rate mixes with the glassy PLA with a high degradation rate, the blend can show better toughness and the tensile strength increases. Thus, blending them together is one of the efficient strategies for creating a new biocompatible blend [35]. The property supplementary between these two biocompatible polymers is very important to their blend materials.

From the literature review of polymer blends, the reason behind the dependence of phase morphology on shape memory properties and also, the shape memory mechanism are still not clear [36]. So, we fabricated a new type of triple-shape memory polymer blend, which can be easily prepared to achieve superior shape memory properties. This blend includes two immiscible ingredients with a well-separated transition temperature. To study the shape memory mechanism, the samples were prepared with various phase morphology due to their immiscibility.

This study is motivated by the current research in the field of MSMPs that have biomedical applications. In this work, the PLA/PCL blends with various composition ratios were prepared by solution mixing and by introducing cross-linking linkages. The switching temperatures were chosen based on the melting points of the two phases. The influence of the blend ratio on the morphology, thermal properties, and

triple-shape memory behavior was studied and discussed in detail.

Experimental

Materials

Poly (L-lactide) (PLA) was supplied by NatureWorks. LLC., USA (grade 3251D, D-isomer ˂ 2%, $M_n = 123,000$ g mol^{-1}, $M_w = 218,000$ g mol^{-1}) with a MFI = 35 g/10 min and density = 1.24 g cm^{-3}. Poly (ε-caprolactone) (PCL) was supplied by Sigma-Aldrich (grade 200, $M_n = 80,000$ g mol^{-1}, $M_w = 97,000$ g mol^{-1}). *N,N*-Dimethylformamide (DMF) was purchased from Merk Chemical Co. and was dried using a solvent purification system from Glass Contour. Dicumyl peroxide (DCP), used as a radical initiator, was supplied by Hercules Korea Chemical Co., Ltd and the triallyl isocyanurate (TAIC) used as a cross-linker was purchased from GO YEN Chemical Industrial Co., Ltd., Taiwan.

Sample Preparation

The binary PLA/PCL blends were obtained as described: before the solution-blending, the PLA and PCL were dried overnight under vacuum at 80 °C and 50 °C, respectively, to minimize the water content. Typically, the PLA/PCL blends with a concentration of DCP (1.5 wt%) and TAIC (2 wt%) were prepared by using DMF as a solvent. The PLA and PCL were completely dissolved in the dry DMF at a concentration of 100 mg ml^{-1} at 70 °C, followed by stirring for 4 h to obtain the homogenous PLA/PCL solution. To obtain well-dispersed radical initiator and cross-linker in the blend, DCP and TAIC were at first dissolved in absolute and dry DMF and then, added to the blend. After that, the solvent was evaporated at high temperature for about 3 h, and then the blend film was obtained. The film was further dried at 50 °C in a vacuum oven for 4 days to remove the solvent completely. Three different PLA/PCL formulations were prepared. The mass ratios of the prepared samples were 70/30, 50/50, and 30/70, denoted as PLA70/PCL30, PLA50/PCL50 and PLA30/PCL70. The melt-processed blends were then molded as a sheet for the DMA analyses (typical thickness 1 mm) by compression-molding with the following procedure to suppress any bubbles: drying at 50 °C overnight, preheating at 150, 170 °C for 5 min, then 10 min at 80, 190 °C at 30 MPa, and cooling at 0 °C.

Characterization

Differential scanning calorimetry (DSC) measurements were performed using a DSC 2010 from TA Instruments under nitrogen flow. The melting temperature and the degree of

crystallinity of PLA were evaluated with the following procedure: the sample was first heated at a rate of 5 °C min^{-1} to 250 °C, kept at this temperature for 5 min to erase any thermal history, and cooled to -30 °C at a cooling rate of 5 °C min^{-1}. The sample was then reheated at a rate of 5 °C min^{-1} to 250 °C. The melting temperature (T_m) was determined at the inflection point. The degree of PLA crystallinity (X_c) was measured by deducing the cold crystallization enthalpy (ΔH_{cc}) to the melting enthalpy (ΔH_m), normalized by the PLA amount (w) in the sample, and by considering a melting enthalpy of 93 J g^{-1} for 100% crystalline PLA (ΔH_0) [34, 35].

$$\% \, X_c = \frac{\Delta H_{m-} \Delta H_{cc}}{w \times \Delta H_0} \times 100 \tag{1}$$

The gel content (G%) was determined by the amount of insoluble material in chloroform, using the following steps (since the standard for determining the G% of the PLA/PCL blend is not available, we had to use the standard of PE for measuring the gel content of the blends): all the samples were cut into pieces, then swollen and extracted with chloroform at room temperature for 72 h. The masses of the original samples (m_o) and the dried, extracted samples (m_d) were recorded. The gel content was calculated by following formula [37].

$$G\% = \frac{m_d}{m_o} \times 100 \tag{2}$$

The morphological fracture of the unetched samples was investigated by using a scanning electron microscope (SEM) (VEGA-Π, XMU, Tescan, Czech Republic) with 20 kV accelerating voltage. To reach the brittle fracture, the sheet samples were broken in liquid nitrogen.

The fractured surfaces of the samples were also etched with acetic acid for 24 h at room temperature, in order to dissolve the PCL phase in the samples containing 50% and 70% PCL. For the sample containing 30% PCL, dichloromethane was used to dissolve the PLA phase. The morphologies were also investigated by using a Nova NanoSEM 450 field emission gun SEM (FEG-SEM), (FEI, USA) with 15 kV accelerating voltage.

A sputter coater was used for both samples, to coat the fractured surface with gold for enhancing conductivity.

The X-ray diffraction (XRD) analysis was performed on a Philips X'Pert PRO Diffractometer with Cu (Kα) radiation. The XRD spectra were recorded at 40 kV and 10 mA with scanning angle from $2\theta = 10–40°$ at a scanning speed of 2° min^{-1}.

For triple-shape memory testing, a shape memory characterization of the samples was cut from the compression-molded sheets into rectangular specimens of approximately 20 mm × 5 mm × 1 mm dimensions. All the thermomechanical cycles were carried out with a stress-controlled DMA Q800 from TA Instruments, in film tension mode. The test program in triple-shape memory effect (TSE) cycle is schematically illustrated in Fig. 1. In step 1, the sample (shape A) was first heated to a high temperature T_{high} (165 °C) and kept for 10 min under a low tensile stress of 0.001 N to allow stress relaxation before extending. Then, the stress-controlled uniaxial stretching was applied. The stress was kept constant during subsequent quenching. In step 2, the

Fig. 1 The thermo-mechanical cycles of the triple-shape memory effect (TSE) of the PLA/PCL blend
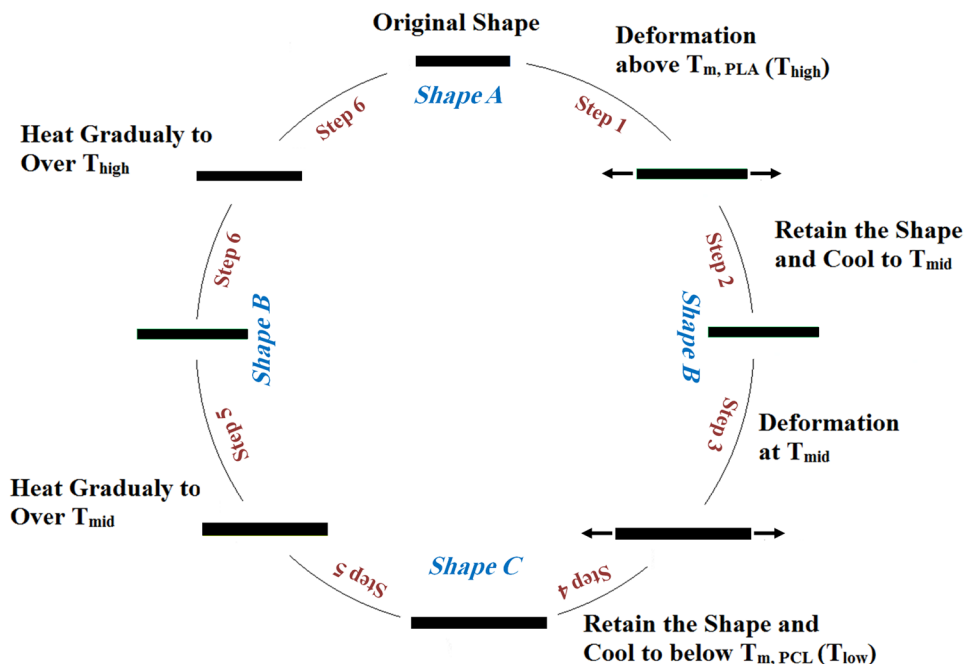
sample was cooled to a middle temperature T_{mid} (70 °C) to fix the first temporary shape obtained in step 1. After the release of the external stress, the sample reached a shape B. In step 3, similar to step 1, after being kept for another 10 min at T_{mid} the sample was extended again. In step 4, after cooling the sample to a low temperature T_{low} (0 °C), a shape C was obtained upon releasing the stress. In step 5, a free strain recovery was performed under continuous reheating to T_{mid} at 5 °C min^{-1} to return to shape B. Finally, in step 6, when the sample was further reheated to T_{high}, its original shape was recovered. The six TSE cycles were examined. The shape fixity ratio R_f and shape recovery ratio R_r were calculated according to Eqs. 3–7 [38].

$$(\%) \, R_{f, \, A \to B} = \frac{\varepsilon^1_{f \, (N)} - \varepsilon^2_{p \, (N-1)}}{\varepsilon^1_{d \, (N)} - \varepsilon^2_{p \, (N-1)}} \times 100 \qquad (3)$$

$$(\%) \, R_{f, \, B \to C} = \frac{\varepsilon^2_{f \, (N)} - \varepsilon^1_{f \, (N)}}{\varepsilon^2_{d(N)} - \varepsilon^1_{f \, (N)}} \times 100\% \qquad (4)$$

$$(\%) \, R_{r, \, C \to B} = \frac{\varepsilon^2_{f \, (N)} - \varepsilon^1_{p \, (N)}}{\varepsilon^2_{f \, (N)} - \varepsilon^1_{f \, (N)}} \times 100\% \qquad (5)$$

$$(\%) \, R_{r, \, B \to A} \frac{\varepsilon^1_{f \, (N)} - \varepsilon^2_{p \, (N)}}{\varepsilon^1_{f \, (N)} - \varepsilon^2_{p \, (N-1)}} \times 100\% \qquad (6)$$

$$(\%) \, R_{r, \, C \to A} \frac{\varepsilon^2_{f \, (N)} - \varepsilon^2_{p \, (N)}}{\varepsilon^2_{f \, (N)} - \varepsilon^2_{p \, (N-1)}} \times 100\% \qquad (7)$$

Here $\varepsilon^2_{p(N-1)}$ is equal to the original strain ($\varepsilon_{p(0)}$) of shape A. $\varepsilon^1_{d(N)}$ is the engineering strain after uniaxial stretching in step (1) $\varepsilon^1_{f(N)}$ is the engineering strain of shape B after unloading in step (2) $\varepsilon^2_{d(N)}$ is the engineering stain after uniaxial stretching in step (3) $\varepsilon^2_{f(N)}$ is the engineering strain of shape C after unloading in step (4) $\varepsilon^1_{p(N)}$ is the engineering strain of recovered shape B in step 5 and $\varepsilon^2_{p(N)}$ is the engineering strain of original shape (shape A) in step 6.

Results and Discussion

Cross-Linking Linkage

Cross-linking linkage can occur in the amorphous segments of semi-crystalline polymers [39, 40]. Therefore, there is a great opportunity for the cross-linking of polymeric chains in the mobile amorphous phase, to be obtained when there is a time delay between the formation of the crystallites and the beginning of the cross-linking reaction [41]. TAIC is widely used as an efficient cross-linking agent. It can generate radicals when its double bond is broken and the polymer networks can be obtained by free-radical cross-linking. By adding DCP to the blend in presence of TAIC, proxy radicals are formed by the decomposition of DCP. Then, the proxy radicals absorb the hydrogen of the PLA and PCL chains in order to form macroradicals of them. The double bonds of the allyl groups in TAIC are cut off and between the PLA and PCL molecules, the chemical cross-links are formed simultaneously [42, 43]. In order to confirm the formation of the cross-linking linkage in the PLA/PCL phases, the gel content tests were carried out. The G% of the samples is listed in Table 1. As can be seen, all the samples showed approximately the same gel content ($\approx$ 98%), meaning that the cross-linking had been successful in the samples. In addition, it seems that the PLA phase had a better response to the applied cross-linking system. Cross-linking the PLA chains in the amorphous phase increased the cross-linking linkages at the ends of the chain and prevented them from decomposition at the melting point. It also helped preserve large amounts of the long crystallizable PLA segments in the beginning of the crystallization in order to increase the crystallization ability in the cooling cycle [40, 42], while in the crystalline phase, the chain segments do not take part in the reaction.

Phase Morphology

It is useful to start with a description of the morphology of the phases due to its crucial rule in other properties. Figure 2 shows the SEM micrographs of the fractured surfaces of the various PLA/PCL blends in etched and unetched forms. As can be seen in Fig. 2a, the domain and morphology of the sample containing 70 wt% PLA is a droplet-matrix with droplets of the PCL dispersed in the continuous matrix of PLA. The average size of the dispersed particles was around 5 μm and its distribution is shown in corner of the image. Due to the immiscibility between the two components, the sample showed the phase separation and clear, weak interfacial adhesion. The same morphology was reported in previous works [33, 35]. With increasing the PCL content to 50 wt%, the PCL phase would turn from a droplet-like

Table 1 The gel content results of the prepared PLA/PCL blends

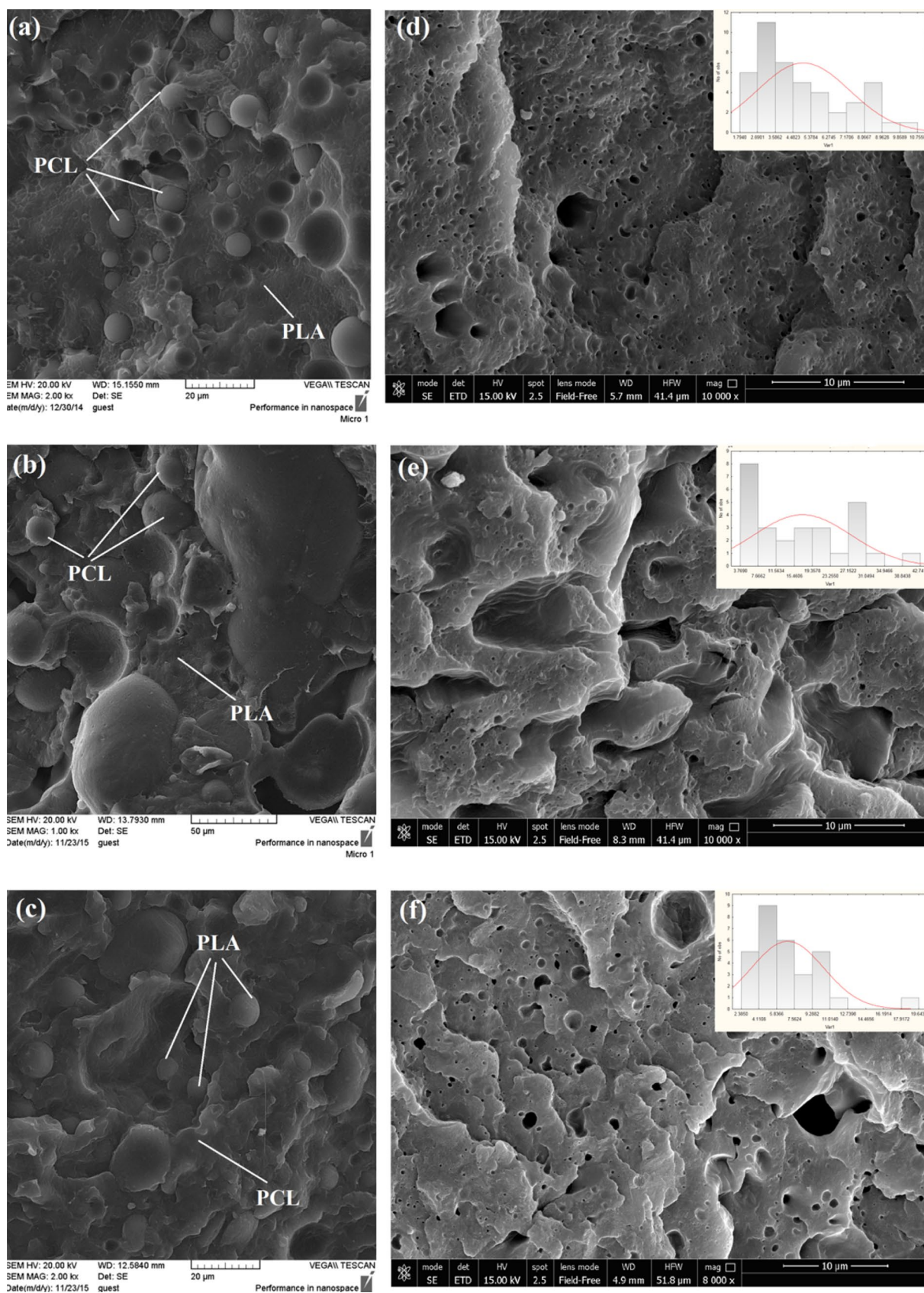| Sample name	Gel content (%)
PLA70/PCL30	99.5
PLA50/PCL50	98.7
PLA30/PCL70	97.2

Fig. 2 The SEM images of the fractured surfaces of PLA/PCL blends. **a** PLA30/PCL70. **b** PLA50/PCL50. **c** PLA70/PCL30. The left images were for the unetched samples and the right images were FEG-SEM for the etched samples

dispersion phase to a continuous phase. In other words, both continuous and droplet-matrix morphologies were observed. However, it seems that the morphology is more similar to a droplet-matrix with bigger size of spherical droplet phase (Fig. 2b). It is proposed that phase inversion could occur in the region of 50 wt% PLA. In the sample containing 70 wt% PCL (Fig. 2c), the droplets of PLA were dispersed in the PCL matrix and it seems that the phase inversion occurred behind this blend ratio. The phase morphology analysis helps us to understand the triple-shape memory mechanism of the PLA/PCL blends.

Thermal Properties

In this work, the melting temperatures of PLA ($T_{m,PLA}$) and PCL ($T_{m,PCL}$) serve as the transition temperature (T_{trans}) for inducing triple-shape memory. DSC was employed to investigate the thermal behavior of the samples. Figure 3 shows the DSC thermograms of a typical sample of PLA50/PCL50 before and after cross-linking. As can be seen, for the non-cross-linked sample, there are two endothermic melting points of the PCL and PLA crystalline phases. In addition, the cold-crystallization of PLA was also observed for the sample. For the sample containing 50 wt% of PCL, the cold crystallization enthalpy ($\Delta H_{cc,PLA}$) and melting enthalpy ($\Delta H_{m,PLA}$) of the PLA phase and crystalline enthalpy ($\Delta H_{c,PCL}$) of the PCL phase were decreased after cross-linking, and also, there is no crystalline exothermic peak of PLA. It was found that the crystallization behavior of sample is affected by cross-linking, the melting enthalpy and the crystallization enthalpy of the phases decreased after the cross-linking. It means that the PLA crystallization kinetics is low and under the applied test condition, no crystallization
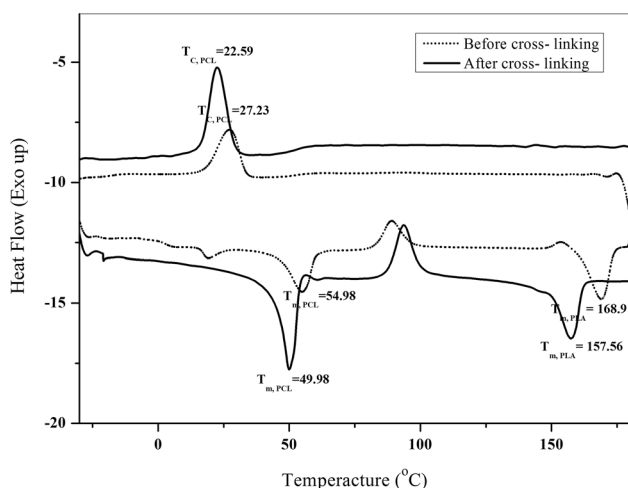
happened. Moreover, the results show that the cross-linking may limit the movements of the chains, which reduces the crystallinity of the phases.

Figure 4 illustrates the DSC curves of the blends with different composition ratio in the cooling (a) and heating scans (b). The obtained data are summarized in Table 2. Considering the cooling step, one can find that there was no crystallization peak of PLA, which means that the incorporation of PCL couldn't enhance PLA crystallization kinetics, as expected. With increasing the content of PCL from 30 to 50 wt%, the melting temperature (T_m) and melting enthalpy (ΔH_m) of both the polymers decreased. At the same time, the change in the exothermic peak of PLA was imperceptible.

Looking at the Table 2, one will find that the crystallization percentage of PLA in the blends is around 5%, indicating the quasi-amorphous state of the material after compression-molding. As shown in Table 2, with increasing the content of the PCL, the crystallinity of PLA decreased,
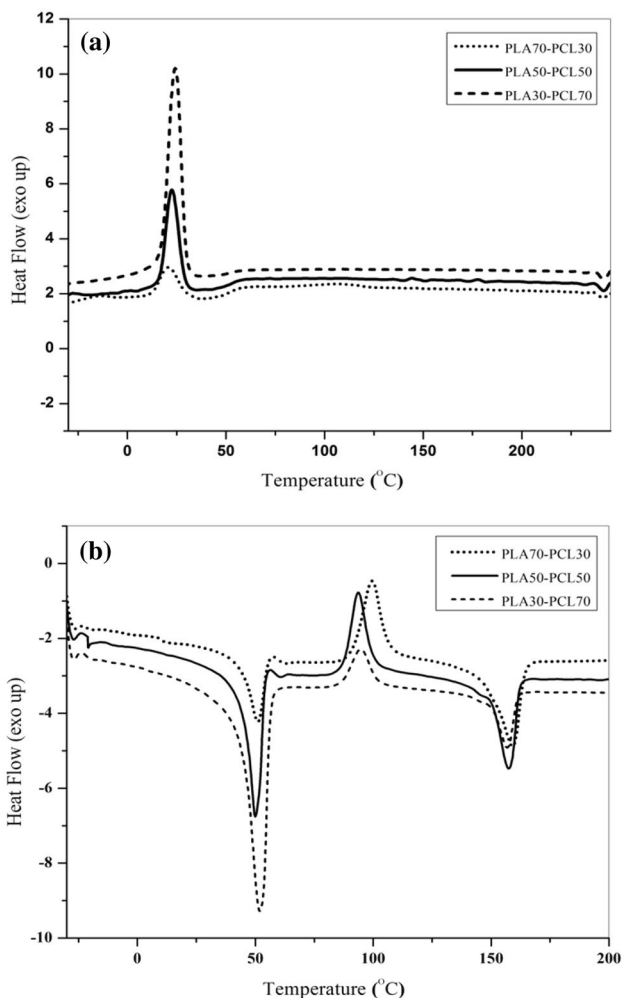

Fig. 3 The DSC curves of typical sample before and after cross-linking (samples with composition ratio 50 wt% PLA act as representative examples)

Fig. 4 The DSC curves of the PLA/PCL blends with different composition: **a** cooling scan and **b** second heating scan. Heating and cooling rate: 5 °C min^{-1}

Table 2 PLA crystallinity and cold crystallinity percentage, the melting temperatures (T_m) and enthalpy of PLA/PCL sheets as a function of PCL content recorded from DSC at 5 °C min^{-1}

% PCL	$X_{c,PLA}$[a] (%)	$T_{m,PCL}$ (°C)	$T_{m,PLA}$ (°C)	$T_{cc,PLA}$ (°C)	$T_{c,PCL}$ (°C)	$\Delta H_{cc,PLA}$ (J g^{-1})	$\Delta H_{m,PLA}$ (J g^{-1})
0	6.99	–	160.03	100.31	–	10.22	12.14
30	5.28	51.08	159.07	99.27	20.77	9.87	11.82
50	1.42	50.98	158.56	97.67	22.59	8.51	9.16
70	1.28	51.86	157.13	94.76	24.28	3.83	4.66
100	–	52.48	–	–	25.67	–	–

[a]Evaluated by the second heating scan, taking into account the relative amount of PLA in the sample and by taking a melting enthalpy of 93 J g^{-1} for 100% crystalline PLA

indicating that the crystallization of PLA is hindered by the presence of PCL, in agreement with the improved miscibility between the phases after increasing the PCL content.

Shape Memory Behavior

As mentioned earlier, the melting points of the crystalline phases were chosen as the transition temperatures (T_{trans}) and triple-shape memory was induced at $T_{m,PCL}$ and $T_{m,PLA}$, which allow them to have two temporary shapes without any interposition. The triple-shape memory properties of all the samples were investigated under a controlled-force mode in film tension. In this section, PLA50/PCL50 was chosen as the typical sample and the programming temperatures were chosen as follows: T_{high} = 165 °C ($T_{m,PLA}$ + 5 °C), which ensures that both the PLA and PCL phases show a good motion in this temperature, T_{mid} = 70 °C ($T_{m,PCL}$ + 15 °C, $T_{cc,PLA}$ − 40 °C),

which certifies that the rigid amorphous fraction (RAF) of the PLA phase controls the movement of the PLA chain compared to the mobile amorphous phase (MAP), which means that there is limited movement due to the lower free volume. The RAF is the consequence of the severe restrictions on the amorphous chain segment mobility, as a result of the fixation of the polymer chain to the crystalline lamella [44]. Unlike the MAP, the RAF does not relax at the glass transition. However, it devitrifies in a temperature region located between the glass transition and the fusion. In the PLA, the devitrification domain of RAF is close to its formation temperature (i.e., the temperature of cold crystallization) [45, 46]. For this reason, we hypothesized that at this temperature (70 °C), the PLA phase is in a glassy state while the PCL phase is in a molten state. T_{low} = 0 °C, at this temperature both the PLA and PCL phases are frosted. The typical triple-shape memory behavior of the sample PLA50/PCL50 is

Fig. 5 Triple-shape memory programming for the sample with two uniaxial stretching at 165 °C and 70 °C and subsequent recovery in continuous heating condition at 5 °C min^{-1} for PLA50/PCL50
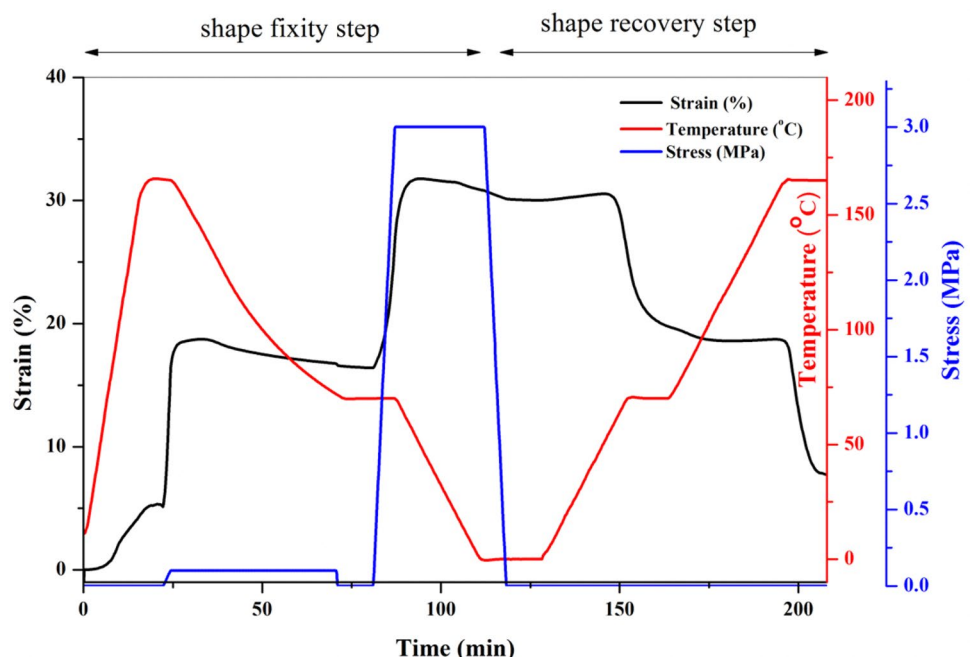
depicted in Fig. 5 in which the variations of strain, stress, and temperature versus time are shown. The results of the triple-shape programmed cycles for all the samples are summarized in Table 3. As can be seen at the first switching point (165 °C), 18% strain was reached under a low constant stress of 0.1 MPa, while at the second switching point (70 °C), the strain was increased by 31% under a high stress of 3 MPa. A stress-free recovery was then performed under continuous heating conditions with isothermal steps at 70 °C and 165 °C. With a careful scrutiny of the recovery cycles, the triple-shape memory behaviors could be derived.

The fixity ratio (R_f) and the recovery ratio (R_r), according to Eqs. 3–7 were determined from these data. From Table 3, we can understand that the R_f and R_r were strongly influenced by the composition ratio of the PCL phase. In the shape fixity program, the R_f of shape A→B ($R_{f,A→B}$) decreased from 93 to 74% and $R_{f,B→C}$ decreased from 91 to 71%, as the PCL content increased from 30 to 70%. $R_{f,A→B}$ is determined by limiting the chain movements of the PLA in the cooling step. It means that by decreasing the content of the PLA, its free volume decreased, so the shape fixity dominates the worse. As for $R_{f,B→C}$, the results corresponded to the crystallization of the PCL phase.

During the recovery, in the first step, with increasing the PCL content, the R_r C→B ($R_{r,C→B}$) increased from 73 to 91% while $R_{r,C→A}$ of all the samples were above 82%. At the second recovery in the fifth and sixth steps ($R_{r,B→A}$), the shape recovery was affected by the PCL phase and decreased with the increase in the PCL content. In other words, at this temperature, the PCL phase is completely melted and decreases the recovery ratio.

Shape recovery from C to B relates to the chain movement of the PCL phase, but the recovery in the second step from B to A shape depends on the flexibility and motion of the PLA phase. The high value of the fixity in these steps is related to the presence of the solidified PLA at this temperature, which helps to fix the applied deformation. This behavior indicates that the PLA/PCL blend could stash triple shapes upon a specific programming step.

The results of the cyclic thermo-mechanical tests are presented in a three-dimensional (3-D) plot of temperature, stress, and strain as X, Y, Z axis respectively for PLA50/PCL50 in Fig. 6.
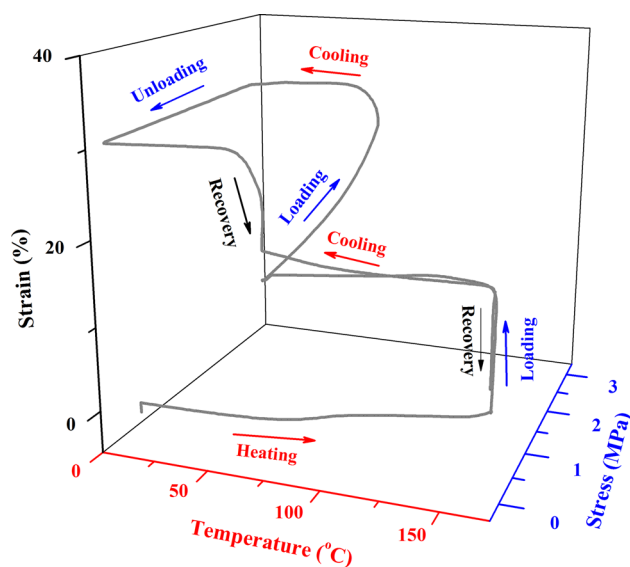

Fig. 6 A representative 3-D plots for cyclic thermo-mechanical result for triple-shape memory behavior of PLA50/PCL50

The Mechanism of Triple-Shape Memory Properties

Figure 7 shows all the imagined schematic variation of the two phases in the triple-shape memory programming for the two obtained morphologies (droplet-matrix and co-continuous). As mentioned in the morphology section, our system had two immiscible phases consisting of soft and hard phases at stretching temperatures. The role of the soft phase with a lower melting point is switching and reversing the temporary shape, while the hard phase with higher melting temperature acts as a fixing phase and determines the permanent shape. These two phases control the shape recovery and shape fixity, respectively.

For the droplet-matrix morphology, at high temperature (T_{high}), both the phases were elongated, while in T_{mid}, the PLA didn't show any significant change and only the PCL was elongated. By cooling the blend to T_{low}, both phases were frozen and were not able to change. At the co-continuous morphology, the same trend of variation was observed for the two phases. Since in this morphology, the two phases co-exist on a larger scale, which effects were highlighted on the triple shape memory behavior.

It can be concluded that for the droplet-matrix (PLA70/PCL30 blend) in Fig. 7a, when the PCL content was too low, the blend exhibited weak shape recovery performance but
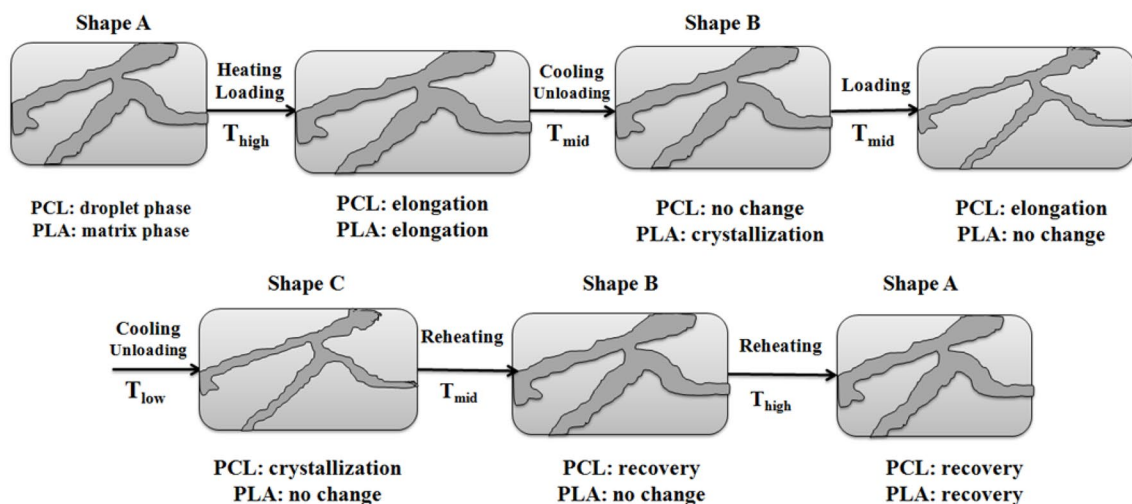
Table 3 Triple-shape memory performance of the PLA/PCL blends recorded from the cyclic thermal mechanical tests carried on DMA	Sample name	$R_{f, A→B}$ (%)	$R_{f, B→C}$ (%)	$R_{r, C→B}$ (%)	$R_{r, B→A}$ (%)	$R_{r,tot, C→A}$ (%)
	PLA70/PCL30	93.42	91.35	73.85	81.76	79.69
	PLA50/PCL50	85.59	88.88	80.49	79.80	89.96
	PLA30/PCL70	74.71	71.63	91.22	73.45	93.54

PLA70/PCL30
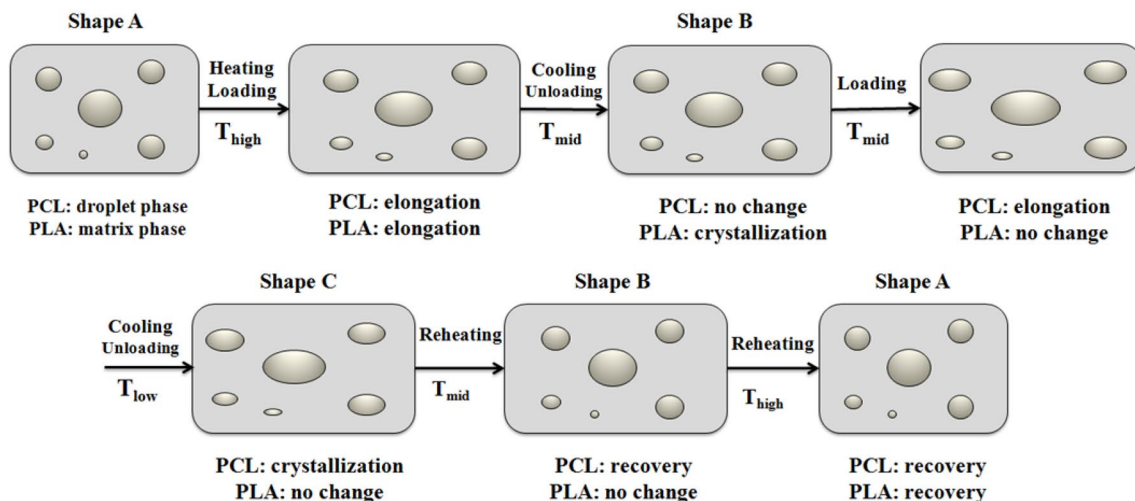
PLA50/PCL50
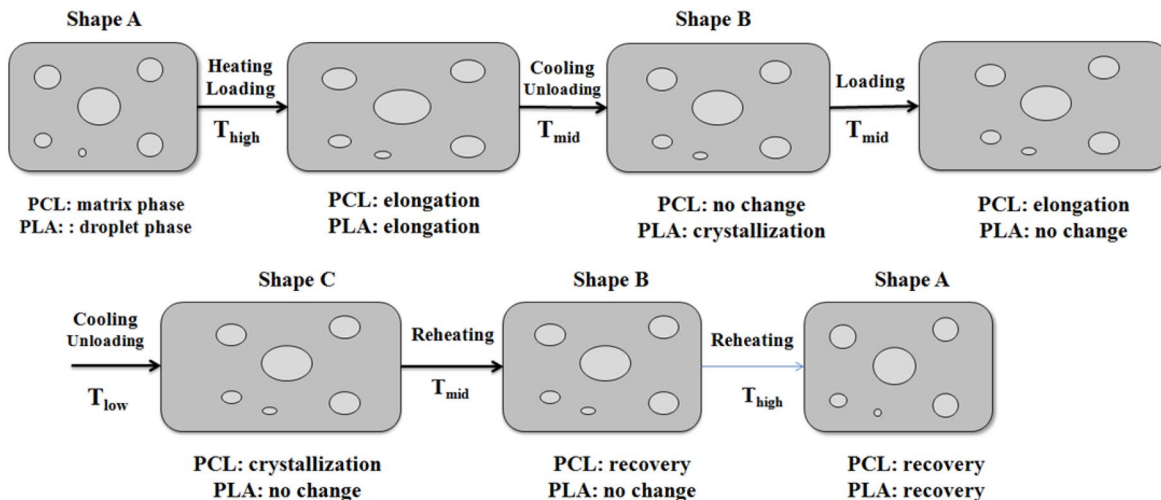

PLA30/PCL70

Fig. 7 The mechanism of the triple-shape memory effect of PLA/PCL blends: PLA70/PCL30, PLA50/PCL50 and PLA30/PCL70

good shape fixity. This indicates that the effect of the reversible phase was small in comparison to the fixed phase, due to its low concentration. In the sample containing a high PCL content (PLA30/PCL70) (Fig. 7c), the blend showed good shape recovery but the deformation was not kept constant and the stress was not stored in the system, leading to bad shape fixity. When the blend ratio was 50/50, the system exhibited the best shape memory properties, which were related to the co-continuous morphology (Fig. 7b).

The X-ray Diffraction (XRD)

The XRD analysis was used in order to obtain a clear evidence for the formation of the crystallites in both the phases. Crystallization has a vital role in the performance of shape memory. So, the status of the crystallinity was monitored at increasing temperatures (at 25 °C, 70 °C, 80 °C, 90 °C, 100 °C and after cooling, at 25 °C again). Figure 8 shows the X-ray diffraction patterns of the samples at the aforementioned temperatures. As can be seen in Fig. 8a, at 25 °C, there are two diffraction peaks at $2\theta = 16.4°$ and $18.6°$, which are correspondent to the PLA crystal and there are two peaks at $2\theta = 21.6°$ and $23.8°$, which are related to the crystalline phase of PCL [33, 47]. With increase in the temperature, the intensities of the peaks related to the PCL decreased and completely disappeared at 100 °C. After cooling, and applying the XRD test at 25 °C, the peaks of the PCL crystalline phases appeared and the intensity of the peaks related to the PLA increased. It can be concluded that the crystallization behavior of the PLA was enhanced at the presence of the PCL and facilitated the shape fixity. This trend was also observed in the other samples. In the sample containing 50 wt% PCL, the decrease in the intensity of the PCL peaks was more than the other samples at a higher temperature. The absence of the crystalline phase of the PCL at this temperature caused better shape recovery in triple-shape memory behavior.

Conclusion

In this study, the cross-linked samples based on the immiscible PLA/PCL blends at different composition ratio were prepared with the solution mixing method in the presence of DCP and with TAIC as a cross-linker. The triple-shape memory effect was induced on the samples and the shape fixity and recovery were determined as the main characteristic indices. The following results can be drawn from this research: the results of the DSC analysis revealed that the crystallization behavior of the PCL and PLA phases was affected by the cross-linking and the composition ratio in the samples. In addition, the appearance of two-separate thermal transition $T_{m,PCL}$ and $T_{m,PLA}$ were confirmed by the
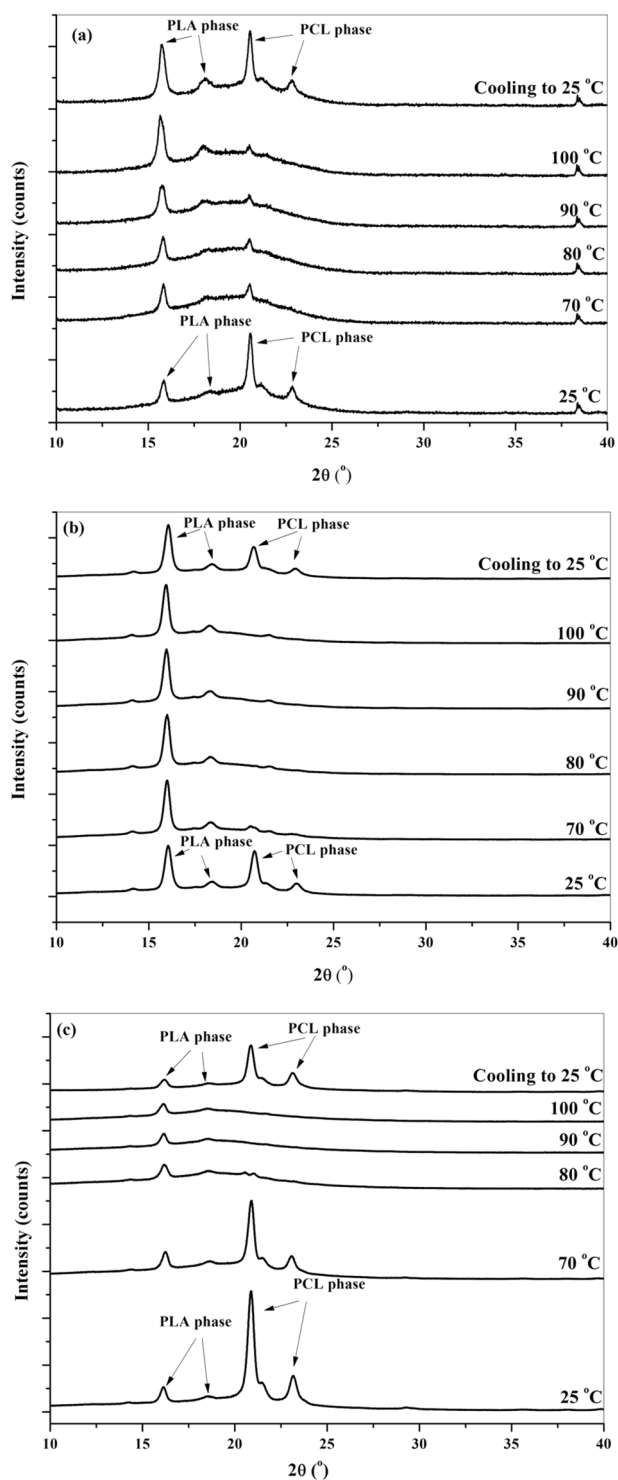

Fig. 8 The X-ray diffraction patterns of **a** PLA70/PCL30, **b** PLA50/PCL50 and **c** PAL30/PCL70 blends at increasing temperatures (25 °C, 70 °C, 80 °C, 90 °C, 100 °C, and 25 °C)

DSC, revealing that the PLA/PCL blends are immiscible in all composition ratios. The SEM micrograph of the samples depicted that the dominant morphology in the samples

PLA70/PCL30 and PLA30/PCL70 was the droplet-matrix type, while in the 50 wt% PCL, a mixture of the droplet-matrix and the co-continuous morphology was observed. The triple-shape memory performance for all the samples was reasonable. The results show that the shape fixity was strongly influenced by the PLA content. However, the shape recovery was affected by the PCL content because of the chain mobility of the PCL phase. From the results, it can be observed that the blend containing 50 wt% PCL demonstrates excellent shape fixity and shape recovery. During the heating–cooling cycle, the level of crystallinity decreased with an increase in the temperature and with further increasing of the temperature, the crystallization peaks of PCL disappeared.

References

1. Lendlin A, Kelch S (2002) Angew Chem Int Ed 41:2034
2. Liu C, Qin H, Mather PT (2007) J Mater Chem 17:1543
3. Abdallah-Elhirtsi S, Fitoussi J, Rashmi BJ, Prashantha K, Farzaneh S, Lacrampe MF, Krawczak P, Tcharkhtchi (2015) Polym Compos 36:1145
4. Memarian F, Fereidoon A, Ahangari MG, Khonakdar HA (2017) Polym Compos. https://doi.org/10.1002/pc.24387
5. Rousseau IA (2008) Polym Eng Sci 48:2075
6. Lei M, Yu K, Lu H, Qi HJ (2017) Polymer 109:216
7. Bae CY, Park JH, Kim EY, Kim BK (2011) J Mater Chem 21:11288
8. Voit W, Ware T, Dasari RR, Smith P, Danz L, Simon D, Barlow S, Marder SR, Gall K (2010) Adv Funct Mater 20:162
9. Zhang S, Yu Z, Govender T, Luo H, Li B (2008) Polymer 49:3205
10. Raquez JM, Vanderstappen S, Meyer F, Verge P, Alexandre M, Thomassin JM, Jerome C, Dubois P (2011) Chem Eur J 17:10135
11. Ortega AM, Yakacki CM, Dixon SA, Likos R, Greenberg AR, Gall K (2012) Soft Matter 8:7381
12. Samuel C, Barrau S, Lefebvre JM, Raquez JM, Dubois P (2014) Macromolecules 47:6791
13. Wang WS, Ping P, Chen XS, Jing XB (2006) Eur Polym J 42:1240
14. Pilate F, Mincheva R, Winter JD, Gerbaux P, Wu L, Todd R, Raquez JM, Dubois P (2014) Chem Mater 26:5860
15. Zhang J, Wu G, Huang C, Niu Y, Chen C, Chen Z, Yang K, Wang Y (2012) J Phys Chem C 116:5835
16. Zhang MQ, Yang KK, Wang YZ (2015) Chin Chem Lett 26:1221
17. Zhang T, Wen Z, Hui Y, Yang K, Zhou Q, Wang Y (2015) Polym Chem 6:4177
18. Pretsch T (2010) Smart Mater Struct 19:015006
19. Behl M, Lendlein A (2010) J Mater Chem 20:3335
20. Bellin I, Kelch S, Langer R, Lendlein A (2006) Proc Natl Acad Sci USA 103:18043
21. Xie T (2011) Polymer 52:4958
22. Zotzmann J, Behl M, Feng YK, Lendlein A (2010) Adv Funct Mater 20:3583
23. Ahn SK, Kasi RM (2011) Adv Funct Mater 21:4543
24. Ware T, Hearon K, Lonnecker A, Wooley KL, Maitland DJ, Voit W (2012) Macromolecules 45:1062
25. Xie T, Page AK, Eastman SA (2011) Adv Funct Mater 21:2057
26. Xie T (2010) Nature 464:267
27. Li J, Liu T, Pan Y, Xia S, Zhang Z, Ding X, Peng Y (2012) Macromol Chem Phys 213:2246
28. Mohanty AK, Misra M, Hinrichsen G (2000) Macromol Mater Eng 276–277:1
29. Mohanty AK, Misra M, Drzal LT (2002) J Polym Environ 10:19
30. Dipa R, Sarkar BK (2001) J Appl Polym Sci 80:1013
31. Sen T, Reddy HN (2013) Adv Mater Sci Eng 2013:1
32. Liao HT, Wu CS (2009) Mater Sci Eng A 515:207
33. Yeh JT, Wu CJ, Tsou CH, Chai WL, Chow JD, Huang CY, Chen KN, Wu CS (2009) Polym Plast Technol Eng 48:571
34. Radusch HJ, Kolesov I, Gohs U, Heinrich G (2012) Macromol Mater Eng 297:1225
35. Wu D, Lin D, Zhang J, Zhou W, Zhang M, Zhang Y, Wang D, Liu B (2011) Macromol Chem Phys 212:613
36. Zhang H, Wang H, Zhong W, Du Q (2009) Polymer 50:1596
37. Xie H, Cheng CY, Du L, Fan CJ, Deng XY, Yang KK (2016) Macromolecules 49:3845
38. Zhao Q, Qi HJ, Xie T (2015) Prog Polym Sci 49–50:79
39. Quynh TM, Mitomo H, Nagasawa N, Wada Y, Yoshii F, Tamada M (2007) Eur Polym J 43:1779
40. Bai H, Liu H, Bai D, Zheng Q, Wang K, Deng H, Chen F, Fu Q (2014) Polym Chem 5:5985
41. Li SC, Liu H, Zeng W (2011) J Appl Polym Sci 121:2614
42. Yang SL, Wu ZH, Yang W, Yang MB (2008) Polym Test 27:957
43. Shayan M, Azizi H, Ghasemi I, Karrabi M (2015) Carbohydr Polym 124:237
44. Androsch R, Wundelich B (2005) Polymer 46:12556
45. Delpouve N, Delbreilh L, Stoclet G, Saiter A, Dargent E (2014) Macromolecules 47:5186
46. Righetti MC, Tombari E (2011) Thermochim Acta 522:118
47. Brizzolara D, Cantow HJ, Diederichs K, Keller E, Domb AJ (1996) Macromolecules 29:191